CHEMISTRY OF MATERIALS

pubs.acs.org/cm Article

# Layer-by-Layer Structural Identification of 2D Ruddlesden–Popper Hybrid Lead Iodide Perovskites by Solid-State NMR Spectroscopy

Jeongjae Lee, Woocheol Lee, Keehoon Kang,* Takhee Lee,* and Sung Keun Lee*

Cite This: *Chem. Mater.* 2021, 33, 370–377 Read Online

ACCESS | Metrics & More | Article Recommendations | Supporting Information

**ABSTRACT:** Application of two-dimensional (2D) organic–inorganic hybrid halide perovskites in optoelectronic devices requires a detailed understanding of the local structural features including the Pb–I bonding in the 2D layers and the organic–inorganic interaction between the organic spacer molecules and the perovskite layer. In this study, we show that $^{1}H$ and $^{207}Pb$ solid-state nuclear magnetic resonance (NMR) spectroscopy can serve as a noninvasive and complementary technique to probe the local structural features of the 2D Ruddlesden–Popper phase $BA_2MA_{n-1}Pb_nI_{3n+1}$ ($n$ = 1–4) with butylammonium (BA) spacers. $^{207}Pb$ echo and $^{207}Pb \rightarrow {}^{1}H$ heteronuclear correlation experiments enable layer-by-layer structural detection of 2D halide perovskites. We show that the observed correlation between $^{207}Pb$ NMR shifts and mean Pb–I bond lengths around each Pb site allows us to probe the local bonding environment of Pb. We envisage that this technique will be vital for a better understanding of the properties of materials as determined by the local atomistic environments in multidimensional halide perovskites.

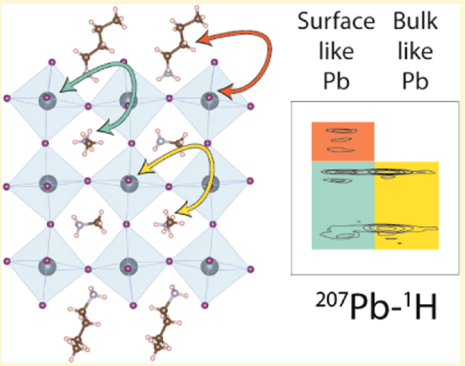


## INTRODUCTION

Since the discovery of metal-halide perovskites (MHPs) as active materials for high-efficiency photovoltaic cells, their outstanding photophysical properties and solution processability have been further exploited in various optoelectronic and electronic device applications.[1−11] One of the most established MHPs is methylammonium lead iodide ($MAPbI_3$) perovskite, the poor stability of which has urged the field to search for a more stable formulation in the vast chemical composition space.

In this regard, Ruddlesden–Popper (RP)-type phases with embedded 2D perovskite layers have recently gained attention due to their superior chemical and photostability.[12−15] These structures have a general formula of $A'_2A_{n-1}M_nX_{3n+1}$, where A′ is an extra aliphatic or aromatic ammonium cation (e.g., butylammonium, $CH_3(CH_2)_3NH_3^+$), A is a small organic cation (e.g., MA), M is a metal ion (e.g., Pb, Sn), and X is a halide ion (e.g., Cl, Br, I). Here, the organic A′ cations act as spacer layers for encapsulating the two-dimensional networks comprising $n$ layers of perovskite polyhedra.[16−18] In addition to their role as protecting the perovskite layers, the organic spacer layer provides an extra degree of freedom for modulating the local atomic structure and the interlayer coupling between the inorganic perovskite layers,[19−22] both of which dictate the transport and optoelectronic properties of the 2D hybrid perovskites. Thus, it is essential to develop an experimental toolkit for determining this organic–inorganic interaction of 2D perovskite-derived RP phases on an atomic scale[23−26] to better understand their highly tunable physical properties coupled to the structures.[14,27,28]

Multinuclear nuclear magnetic resonance (NMR) spectroscopy is a powerful tool for examining the bulk- and surface-specific structures of materials. In addition to being a noninvasive technique unlike X-ray or electron-based methods,[29] NMR has been proven useful for probing the local bonding and molecular motion in many functional materials including batteries, polymers, and MHPs,[30−37] where the local structures of not only strong X-ray scattering (heavy) elements (e.g., Pb as in this work or Sn[38,39]) but also weak X-ray scattering (light) elements (e.g., H, Li, C) are important to their functionality. The strength of NMR as a structural analysis technique lies in this ability to probe the structure and dynamics of both heavy and light elements, not to mention the ability to probe the interaction between them through heteronuclear correlation experiments. Therefore, in the context of hybrid RP phases, NMR is a unique technique for determining not only the structures of the organic spacer and inorganic MHP layers but also their interaction between the spacer ligand and the inorganic metals. As many key physicochemical properties of these 2D perovskites are determined by this interlayer coupling, establishing a baseline for this layer-by-layer detection approach[40] is crucial for

Received: October 19, 2020
Revised: December 10, 2020
Published: December 28, 2020







https://dx.doi.org/10.1021/acs.chemmater.0c04078
*Chem. Mater.* 2021, 33, 370–377

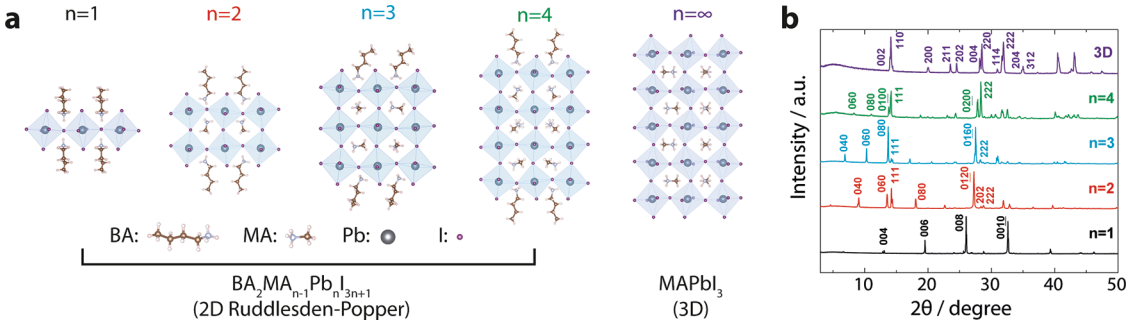


**Figure 1.** (a) Schematic structures of the 2D Ruddlesden−Popper $BA_2MA_{n-1}Pb_nI_{3n+1}$ ($n$ = 1−4) and 3D $MAPbI_3$ perovskites considered in this study. (b) Powder X-ray diffraction data for the prepared crystalline phases with labeled Miller indices for each reflection[44,45] present in the structure.

characterizing the structure and dynamics of each layer in 2D perovskite phases, especially for, e.g., perovskites with mixed organic spacers that are difficult to characterize via diffraction techniques.[41−43]

Here, we show that a combined $^{207}$Pb and $^{1}$H multidimensional solid-state NMR can be useful for determining the composition and local structural features of 2D RP phases with lead iodide perovskite layers. 1D NMR spectra could be used to identify each Pb and H sites. $^{207}$Pb−$^{1}$H 2D heteronuclear correlation (HETCOR) experiments show the spatial proximities between each Pb and H sites, thus allowing us to reveal the structure and dynamics of the organic and perovskite components in RP phases.

## RESULTS AND DISCUSSION

**X-ray Diffraction.** Crystal structures and powder X-ray diffraction patterns for pulverized single crystals of both 2D RP and 3D lead iodide perovskites, $BA_2MA_{n-1}Pb_nI_{3n+1}$ ($n$ = 1−4; BA = butylammonium and MA = methylammonium), and 3D $MAPbI_3$ are shown in Figure 1 (see the Supporting Information for details on the preparation[44,45]). All of the samples show diffraction peaks that match well with previously reported reflections (Figure 1b).[14,44,46]

**$^{1}$H and $^{13}$C NMR.** We start by presenting the $^{1}$H and $^{13}$C solid-state NMR spectra of these 2D hybrid perovskites. For the parent 3D $MAPbI_3$ and 2D layered structures ($n$ = 2−4), the $^{1}$H peaks arising from the MA (6.36 and 3.43 ppm) and BA (6.84, 3.84, 2.19, 1.69, and 1.17 ppm) cations can be assigned (Figure 2a).[17,47] Similarly, $^{13}$C peaks for MA (30.3 ppm) and BA (44.0, 31.2, 20.9, 15.8 ppm) are well identified (Figure S4).

Upon further reduction in the perovskite layer thickness to the $n$ = 1 sample ($BA_2PbI_4$), the MA peaks are no longer visible as expected for this stoichiometry. At the same time, however, the BA peaks broaden significantly and the ammonium resonance ($-NH_3^+$) shifts toward a higher frequency (7.18 ppm). This broadening, which is also observed in $^{13}$C direct excitation spectra upon sample heating (Figure S5), is a direct evidence for the alkyl chain disorder/motion in the $n$ = 1 sample, a phenomenon resembling the dynamics of the aromatic spacer cation in a similar $n$ = 1 phase with phenylethylammonium (PEA) spacers;[48] this is discussed in detail in the Supporting Information. We note that ab initio calculations of the $^{1}$H shifts may provide further insights into the hydrogen−halogen interactions present in our system, but this is outside the scope of the current work.

Finally, the quantitative nature of $^{1}$H and especially $^{13}$C solid-state NMR allows us to determine the MA:BA ratio from peak intensities. This allows a direct confirmation of the structural formula for these 2D hybrid perovskites under crystalline conditions,[49] whereas a previous study by Soe et al. have relied on solution-state NMR with dissolved samples in NMR solvents.[17]

**$^{207}$Pb NMR.** Direct excitation $^{207}$Pb MAS Hahn-echo spectra of the 2D and 3D samples are presented in Figure 2b; static $^{207}$Pb echo spectra were also collected and are shown in Figure S6. Observed isotropic shifts for each Pb site are summarized in Table 1.

The 2D perovskite structures can be considered as being composed of "outer" Pb layers near the organic spacers (i.e., like in $n$ = 1) and "inner" Pb layers (i.e., like in 3D) in different proportions;[18] in the following, we use the above labeling for structural discussion. Using this labeling, peak assignments for the bulk-like 3D and surface-like $n$ = 1 cases are straightforward as only a single crystallographically distinct Pb site exists for these structures.

For the 2D perovskites ($n$ = 1−4), a general trend of increasing shifts for the surface-like Pb sites (Figure 2b, yellow dashed line) is observed, whereas the bulk-like Pb sites (Figure 2b, purple dashed line) retain similar shifts to the 3D $MAPbI_3$ case. This similar shift clearly shows the 3D-like nature of the inner Pb sites relative to the surface-like outer Pb sites subjected to the BA encapsulation. This allows us to clearly distinguish between the Pb sites closer to the ligand (outer) and 3D-like (inner) in 2D perovskites through directly exciting and observing the $^{207}$Pb nuclei. The chemical environment of these outer Pb sites shares similarity with the surface Pb sites in a bulk perovskite crystal, especially as the layer thickness $n$ increases (and theoretically reaches infinity for a bulk crystal). Hence, the ability to distinguish the inner and outer chemical environments shows a potential for extracting information on the surface states such as edge states, which have been shown to play important roles in providing a fast route for exciton dissociation and carrier conduction in 2D hybrid perovskites.[50−52]

More quantitatively, for the $n$ = 3 structure, the outer and inner sites could be identified from approximately 2:1 peak intensities for the 1572 and 1354 ppm resonances (Figure S3a). As the $n$ = 3 structure consists of one 3D-like Pb layer sandwiched between the two outer Pb layers,[17] the 1572 ppm peak should correspond to the outer Pb site.

For the $n$ = 2 and 4 samples, non-centrosymmetric space groups were previously identified through single-crystal X-ray


https://dx.doi.org/10.1021/acs.chemmater.0c04078
Chem. Mater. 2021, 33, 370−377

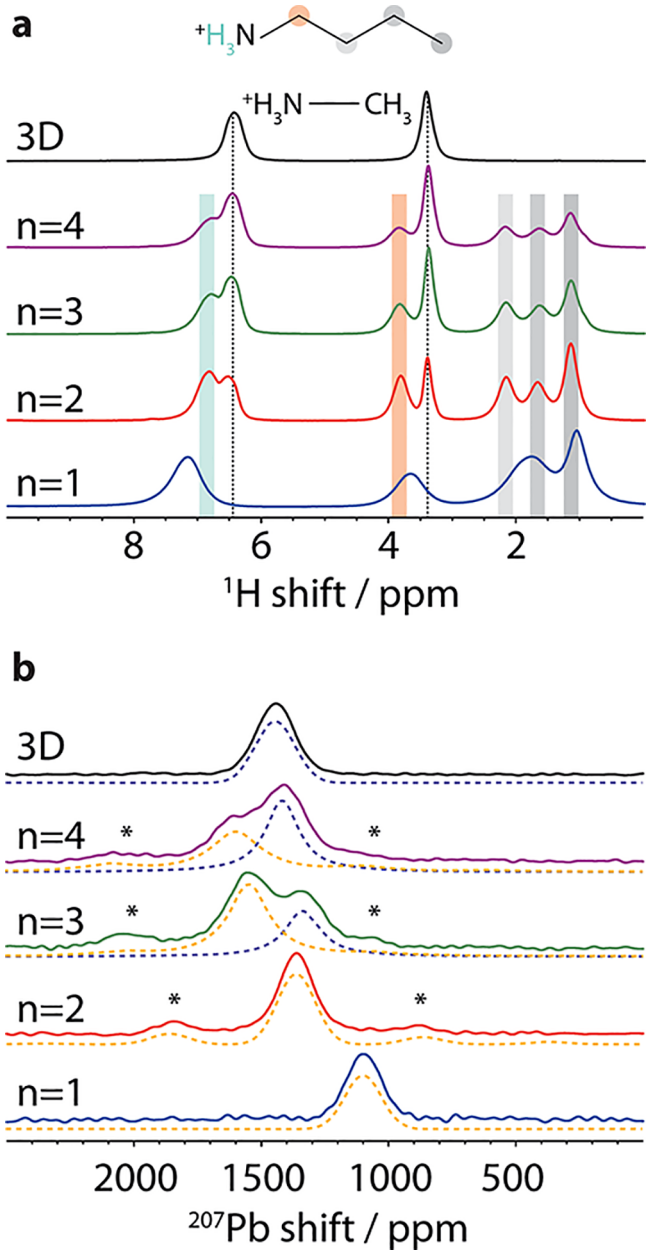


**Figure 2.** Solid-state MAS NMR spectra of 2D $BA_2MA_{n-1}Pb_nI_{3n+1}$ and 3D $MAPbI_3$ perovskites. (a) Quantitative single-pulse $^1H$ spectra taken at 50 kHz MAS. Each H site in the BA molecule is color-coded. (b) $^{207}Pb$ Hahn-echo spectra taken at 62.5 kHz MAS. Spinning sidebands are marked by asterisks (*). Fits to the "outer" (orange) and "inner" (purple) sites are shown in dashed lines.

diffraction and static ab initio calculations,[16,17] signifying that the individual inner/outer layers are nonequivalent on the XRD timescale. For the $n = 2$ sample, however, only a single Pb resonance is observed at 1361 ppm with a similar peak width to the 3D $MAPbI_3$ with a single Pb site (Table S3). As NMR can only probe structures on a ms to $\mu$s timescale, this discrepancy could arise from the NMR probing the time-averaged structure of MA group reorientation and/or $PbI_6$ octahedral motion happening at a much faster timescale than the NMR timescale.[53] Assuming this averaging happens for the $n = 4$ sample, we would then expect to observe two Pb resonances of equal intensity arising from the inner and outer Pb sites, which is indeed the case from the fitted $^{207}Pb$ static and MAS spectra (Figures S3b and S6); this motional equivalence is discussed in detail in the Supporting Information.

Finally, the fitted static spectra (Figure S6) clearly illustrate the existence of nonzero chemical shift anisotropies (CSAs) for the outer lead atoms (all Pb sites in $n = 1$ and 2, and the outer Pb sites in $n = 3$ and 4) all with an axially symmetric CSA tensor ($\eta = 0$). As nonzero CSA arises from aspherical electron charge distribution around the nucleus, this parameter can be used as a proxy to directly probe the octahedral distortion of a $PbI_6^{4-}$ moiety arising from the $6s^2$ lone pair in $Pb^{2+}$ atoms; this octahedral distortion is known to play a key role in determining the optoelectronic properties of perovskite materials.[54,55] Empirically, magnitudes of the CSA can be approximately correlated to the "span" of the local Pb−I bonds (defined as the range between the shortest and longest Pb−I bond lengths)[56] as shown in Table 1; for further discussion see the SI.

**$^{207}Pb \rightarrow {}^1H$ HETCOR.** To aid the assignment of the overlapping outer and inner peaks for the $n = 3$ and $n = 4$ samples, $^1H$-detected $^{207}Pb \rightarrow {}^1H$ heteronuclear correlation (HETCOR) experiments were performed on these samples. Cross polarization (CP) sequence based on the Hartmann−Hahn matching was used for transferring the initial $^{207}Pb$ polarization to neighboring $^1H$ spins, thus affording 2D correlation spectra between the two nuclei.

Figure 3 shows the $^{207}Pb \rightarrow {}^1H$ HETCOR spectra for all of the 2D samples. Starting with the $n = 1$ and $n = 2$ samples, the single Pb resonance in each case is shown to be correlated to all of the BA/MA protons, regardless of their distances to the nearest Pb atom (Figure 3a,b). This initially proves that correlations from outer Pb to the BA protons are indeed well visible under our experimental conditions; the extended range of correlation over 6−7 Å (i.e., the spatial separation between outer Pb and the furthest away BA protons) is most likely arising from the relatively long CP contact time (4 ms), during which $^1H - {}^1H$ spin diffusion can take place within the BA molecule. This is supported by the comparable $^1H$ intensities between the direct and spin-diffused CP transfer simulations assuming static cations (Figure S2).

Figure 3c,d shows the $^{207}Pb \rightarrow {}^1H$ HETCOR spectra for the $n = 3$ and $n = 4$ samples. As the outer Pb sites are effectively sandwiched between the MA and BA layers, the correlation between the BA -$CH_2CH_2CH_3$ alkyl chain (marked as gray on plot) and the higher frequency resonances (marked as orange on plot) clearly demonstrates that these peaks correspond to the outer Pb sites. The presence of this correlation is also consistent with the fitted result of the static and MAS $^{207}Pb$ spin echo spectra, where the higher frequency resonances were assigned to the outer Pb based on the intensity argument.

Interestingly, the $^1H$-detected $^{207}Pb$ spectrum (black line on top of Figure 3c) shows a significantly reduced intensity for the outer Pb resonance when compared to the $^{207}Pb$ direct spin echo spectrum (red line). This indicates that more efficient CP transfer occurs from the inner 3D-like Pb atoms than the outer Pb atoms, as $^1H$-detected HETCOR experiments exclusively measure the polarization transferred from the nearby Pb spins. This significant difference in CP efficiency most likely arises from the larger $^{207}Pb$ CSA of the outer Pb sites (Table 1; also see the Supporting Information for further discussion). Unlike the outer Pb sites, the 3D-like inner Pb sites are sandwiched between two MA layers; hence, a strong correlation of the lower frequency peaks (marked as purple on plot) to the MA


https://dx.doi.org/10.1021/acs.chemmater.0c04078
Chem. Mater. 2021, 33, 370−377

Table 1. Summary of Observed $^{207}$Pb Shifts for 2D RP $BA_2MA_{n-1}Pb_nI_{3n+1}$ and 3D $MAPbI_3$ Perovskites.[a]

| site | | nature | average, $d_{Pb-I}$ (Å) | $^{207}$Pb, $\delta_{iso}$ (ppm) | $^{207}$Pb, $\Delta\delta$ (ppm) | $^{207}$Pb, $\eta$ | span (Å) | SSB? |
|---|---|---|---|---|---|---|---|---|
| $n$ = 1 | | | 3.189 | 1084 | −207 | 0 | 0.052 | no |
| $n$ = 2 | Pb1 | MA-CH3 | 3.165 | 1410 | −443 | 0 | 0.168 | yes |
| | Pb2 | MA-NH3 | 3.173 | | | 0 | 0.203 | yes |
| $n$ = 3 | Pb1 | inner | 3.157 | 1354 | 0 | | 0.184 | no |
| | Pb2 | outer | 3.142 | 1572 | −631 | 0 | 0.132 | yes |
| $n$ = 4 | Pb1&2 | inner | 3.161 | 1416 | 0 | | 0.14 | no |
| | Pb3&4 | outer | 3.169 | 1630 | −669 | 0 | 0.32 | yes |
| 3D | 3D | bulk | 3.161 | 1417 | 0 | | 0.071 | no |

[a]Isotropic $^{207}$Pb shift ($\delta_{iso}$) as well as chemical shift anisotropy (CSA) ($\Delta\delta$) and asymmetry ($\eta$) as fitted from static experiments (Figure S6; note the peak positions slightly change under MAS due to frictional heating effects) are also shown following the Haeberlen convention.[57] Span refers to the range of Pb−I distances for each site (i.e., differences between the longest and shortest Pb−I distances).[16,17] SSB refers to the presence of spinning sidebands.

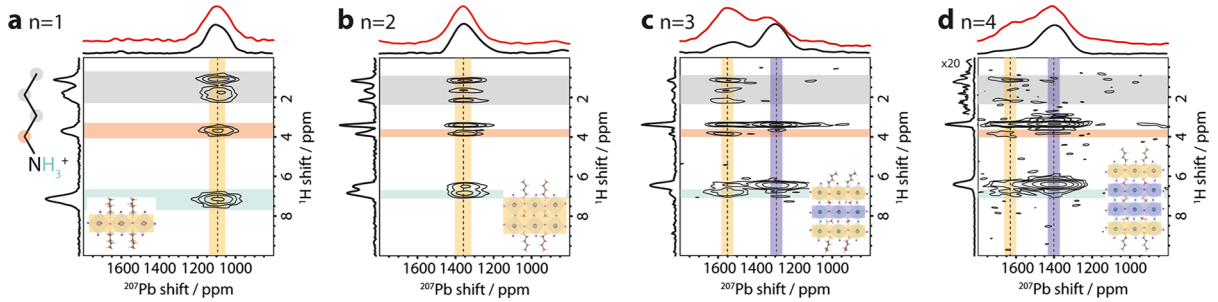


Figure 3. $^1$H-detected $^{207}$Pb → $^1$H spectra for $BA_2MA_{n-1}Pb_nI_{3n+1}$ samples. All experiments were conducted under 62.5 kHz MAS and CP contact time of 4 ms. Overlaid in red are $^{207}$Pb direct polarization spectra taken from Figure 2. Each environment is color-coded for visual aid.

protons signifies that these resonances come from the inner Pb, again in good agreement with the MAS and static $^{207}$Pb data.

**Trends in $^{207}$Pb Isotropic Shifts for Pseudo-Octahedral $PbI_6^{4-}$ Systems.** The well-known utility of NMR spectroscopy lies in the ability to distinguish between different chemical environments in terms of chemical shift dispersion. However, it is often challenging to identify the nature of a given peak solely from the value of its chemical shift (as was the case for the $n$ = 3 and $n$ = 4 samples in this study). Thus, a correlation between the chemical shift and structural properties (e.g., bond distances, bond angles) is of benefit for a quick interpretation and rationalization of the obtained NMR spectra.

Figure 4 shows the plot of the $^{207}$Pb isotropic shift (static) against the average Pb−I bond distance (obtained from previous single-crystal X-ray diffraction studies[16,17]) in 2D and 3D perovskites as obtained in this study. A clear negative trend exists in the linear fit; strikingly, the trend extends well to solid $PbI_2$, where the structure could be described as stacked 2D sheets of edge-sharing $PbI_6^{4-}$ octahedra.[58,59] A similar negative correlation was previously observed between the mean Pb−O bond length and Pb isotropic shifts,[60] indicating that this trend is general and could be extended to other systems. A detailed discussion on the origin of this relationship based on the Ramsey theory is presented in the Supporting Information.

Linear correlations between chemical shifts and bond distances have been well established in many other systems; examples include ionically bonded $^{23}$Na−O,[61,62] covalently bonded $^{29}$Si−O and $^{13}$C−I,[63,64] hydrogen-bonded O-$^1$H...O,[65] and halogen-bonded P=$^{77}$Se···I.[66] Our result suggests that this correlation could be extended to match the Pb−I system with good agreements. As many structural and functional properties such as band structures depend on the nature of local Pb−I bonding, this result provides us with a tool to probe the local

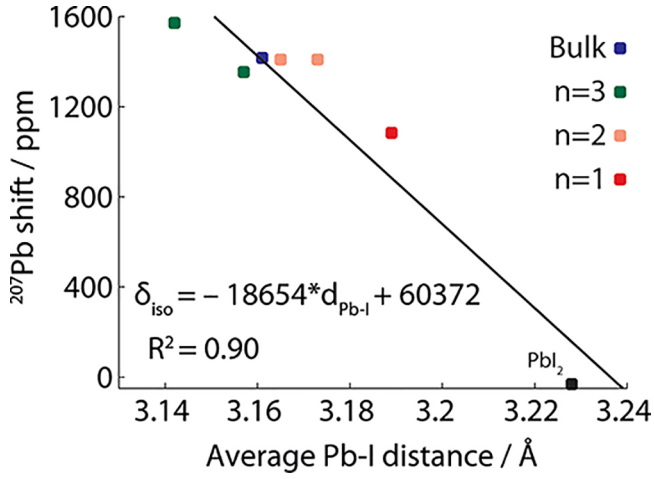


Figure 4. Plot of $^{207}$Pb isotropic shift (static) versus average Pb−I distance of 3D and 2D ($n$=1,2,3) perovskites in this study. The $n$ = 4 sample was omitted in the fit as only a broad distinction between the inner and outer sites could be made. Static $PbI_2$ shift is given by Taylor et al.[58] The reported structure was determined from a single-crystal XRD of the 2H polytype.[59]

chemical environment of Pb via its $^{207}$Pb NMR shift. As NMR is a noninvasive technique that works equally well in the absence of structural periodicity, the present relationship could be useful, for instance, for identifying and rationalizing $^{207}$Pb NMR shifts in novel and/or disordered systems; see the Supporting Information for further discussion.[67] Further extensions of this correlation to other halides with different halide anion components (e.g., Pb−X where X=$Cl^-$, $Br^-$) and other metal cation components (e.g., M−X, where M= $Sn^{2+}$) would also be possible. Application to other 2D hybrid


https://dx.doi.org/10.1021/acs.chemmater.0c04078
Chem. Mater. 2021, 33, 370−377

perovskite phases adopting Dion–Jacobson, Aurivillius, and alternating cation perovskite structures could also be envisaged.[68,69]

## CONCLUSIONS

In conclusion, through the combined solid-state NMR methodology of $^{207}$Pb and $^{1}$H nuclei, layer-by-layer detection and quantification of individual Pb layers in 2D Ruddlesden–Popper phases with hybrid lead iodide perovskite layers are enabled. $^{207}$Pb → $^{1}$H HETCOR allows distinction of the 3D-like "inner" and surface-like "outer" Pb sites in the 2D perovskite layer through spatial correlation between the MA/BA protons and Pb spins. This unique ability of solid-state NMR allows us to probe the nature of organic ligand–inorganic surface interaction, providing insights into the local atomistic structure and dynamics in these systems. The observed linear dependence of $^{207}$Pb isotropic shift and mean Pb–I distance yields a first predictive relationship between the two parameters, therefore offering possibilities for extending this methodology for novel inorganic Pb halide systems. We believe the methodology and understanding presented in this work can potentially be extended to provide insights toward understanding the relationships between highly tunable local structures and properties of other 2D perovskite systems; our work also sheds light on a new opportunity to probe structural changes upon surface-initiated degradation or local creation of novel phases in layered perovskites.

## MATERIALS AND METHODS

**Material Synthesis.** The chemicals used for single-crystal syntheses were purchased as the following: PbO (>99.9%) from Sigma-Aldrich, n-butylammonium iodide (BAI, >99.5%) and methylammonium iodide (MAI, >99%) from Greatcell Solar, hypophosphorous acid ($H_3PO_2$, 50% w/w aq. soln.) from Thermo Fisher Scientific, and hydroiodic acid (HI, 57% in water). For the crystal synthesis of $BA_{2n}MA_{n-1}Pb_nI_{3n+1}$ ($n$ = 1–4), PbO, BAI, and MAI were dissolved in mixed acid solutions of HI and $H_3PO_2$ according to the recipes provided by Li et al.[45] For the synthesis of $MAPbI_3$, we mixed an equimolar ratio of MAI (1.90 g) and PbO (2.66 g) in a mixed acid solution of HI (18 mL) and $H_3PO_2$ (2 mL). The solutions were heated to 130 °C until all of the precursors were dissolved. The solutions were then cooled down to room temperature to precipitate single crystals. All of the crystals were isolated by filtration and dried in vacuo. Structures of the prepared crystals were analyzed by powder X-ray diffraction (Rigaku SmartLab).

**Solid-State NMR Spectroscopy.** All NMR spectra were collected on a 14.1 T Bruker Avance III spectrometer. $^{1}$H and $^{207}$Pb MAS spectra were collected with a Bruker 1.3 mm MAS probe at spinning speeds of 50 and 62.5 kHz. $^{13}$C MAS and $^{207}$Pb static spectra were collected with a Bruker 3.2 mm MAS probe (10 kHz MAS for $^{13}$C). Shifts were referenced to solid adamantane ($^{1}$H 1.87 ppm and $^{13}$C 38.6 ppm) and solid $Pb(NO_3)_2$ ($^{207}$Pb -3474 ppm). For MAS direct excitation experiments (1.3 mm), $^{1}$H and $^{207}$Pb radiofrequency (rf) amplitudes of 200 and 175 kHz were employed, respectively. For direct detection experiments, simple pulse-acquire and rotor-synchronized spin echo experiments were performed for $^{1}$H and $^{207}$Pb, respectively. For $^{1}$H-detected $^{207}$Pb → $^{1}$H HETCOR experiments, Hartmann–Hahn conditions were experimentally optimized with $^{207}$Pb rf amplitude fixed to 100 kHz and a fixed contact time of 4 ms was employed. For $^{13}$C experiments (3.2 mm), 83 kHz rf pulses were used for direct excitation with 70 kHz $^{1}$H SPINAL64 decoupling during the detection period. $^{207}$Pb static spin echo experiments (3.2 mm) were performed with 100 kHz rf pulses and 20 $\mu$s echo delay. Frequency-stepped acquisition was used for $n$ = 3 and 4 samples due to insufficient excitation bandwidth.[70] Experimental details of each data set are reported in the SI (Table S1).

CP transfer efficiency was simulated with the SIMPSON code[71] under identical rf and MAS conditions to the experiment. We note that the large $^{207}$Pb chemical shift anisotropy as fitted in the static spectra would result in a significantly lower transfer efficiency, but this was not included in the simulation. Spectral fitting was performed with the SOLA code as included in Topspin software.

## ASSOCIATED CONTENT

### Supporting Information

The Supporting Information is available free of charge at https://pubs.acs.org/doi/10.1021/acs.chemmater.0c04078.

Supporting information is available on the experimental methods and detailed discussion on the NMR correlation (PDF)

## AUTHOR INFORMATION


### Corresponding Authors

**Keehoon Kang** – *Institute of Applied Physics and Department of Physics and Astronomy, Seoul National University, Seoul 08826, Korea;* orcid.org/0000-0003-1230-3626; Email: keehoon.kang@snu.ac.kr

**Takhee Lee** – *Institute of Applied Physics and Department of Physics and Astronomy, Seoul National University, Seoul 08826, Korea;* orcid.org/0000-0001-5988-5219; Email: tlee@snu.ac.kr

**Sung Keun Lee** – *School of Earth and Environmental Sciences and Institute of Applied Physics, Seoul National University, Seoul 08826, Korea;* orcid.org/0000-0002-3149-3421; Email: sungklee@snu.ac.kr

### Authors

**Jeongjae Lee** – *School of Earth and Environmental Sciences and Institute of Applied Physics, Seoul National University, Seoul 08826, Korea;* orcid.org/0000-0003-4294-4993

**Woocheol Lee** – *Institute of Applied Physics and Department of Physics and Astronomy, Seoul National University, Seoul 08826, Korea*

Complete contact information is available at: https://pubs.acs.org/10.1021/acs.chemmater.0c04078


### Author Contributions

J.L. conceived the idea and carried out the NMR experiments and analyses with assistance from K.K. W.L. prepared the single-crystal samples. T.L. and S.K.L. supervised the project. The manuscript was written through contribution from all authors.

### Notes

The authors declare no competing financial interest.

## ACKNOWLEDGMENTS

This work was supported by the National Research Foundation of Korea (NRF) grants funded by the Korean government (MSIT) (No. NRF-2020R1A3B2079815 and No. 2012026372) J.L. was supported by the National Research Foundation of Korea (NRF) grant funded by the Korean government (MEST) (No. 2019R1A6A1A10073437). K.K. appreciates the financial support by Postdoctoral Science Fellowship from POSCO TJ Park Foundation. We thank the three anonymous reviewers for their helpful comments and insights for improving this manuscript.

## REFERENCES


(1) Lee, M. M.; Teuscher, J.; Miyasaka, T.; Murakami, T. N.; Snaith, H. J. Efficient Hybrid Solar Cells Based on Meso-Superstructured Organometal Halide Perovskites. *Science* **2012**, *338*, 643−647.

(2) Jeon, N. J.; Noh, J. H.; Kim, Y. C.; Yang, W. S.; Ryu, S.; Seok, S. I. Solvent Engineering for High-Performance Inorganic−Organic Hybrid Perovskite Solar Cells. *Nat. Mater.* **2014**, *13*, 897−903.

(3) Kim, M.; Kim, G.-H.; Oh, K. S.; Jo, Y.; Yoon, H.; Kim, K.-H.; Lee, H.; Kim, J. Y.; Kim, D. S. High-Temperature−Short-Time Annealing Process for High-Performance Large-Area Perovskite Solar Cells. *ACS Nano* **2017**, *11*, 6057−6064.

(4) Kim, G.-H.; Jang, H.; Yoon, Y. J.; Jeong, J.; Park, S. Y.; Walker, B.; Jeon, I.-Y.; Jo, Y.; Yoon, H.; Kim, M.; Baek, J.-B.; Kim, D. S.; Kim, J. Y. Fluorine Functionalized Graphene Nano Platelets for Highly Stable Inverted Perovskite Solar Cells. *Nano Lett.* **2017**, *17*, 6385−6390.

(5) Tan, Z.-K.; Moghaddam, R. S.; Lai, M. L.; Docampo, P.; Higler, R.; Deschler, F.; Price, M.; Sadhanala, A.; Pazos, L. M.; Credgington, D.; Hanusch, F.; Bein, T.; Snaith, H. J.; Friend, R. H. Bright Light-Emitting Diodes Based on Organometal Halide Perovskite. *Nat. Nanotechnol.* **2014**, *9*, 687−692.

(6) Cho, H.; Jeong, S.-H.; Park, M.-H.; Kim, Y.-H.; Wolf, C.; Lee, C.-L.; Heo, J. H.; Sadhanala, A.; Myoung, N.; Yoo, S.; Im, S. H.; Friend, R. H.; Lee, T.-W. Overcoming the Electroluminescence Efficiency Limitations of Perovskite Light-Emitting Diodes. *Science* **2015**, *350*, 1222−1225.

(7) Shin, Y. S.; Yoon, Y. J.; Heo, J.; Song, S.; Kim, J. W.; Park, S. Y.; Cho, H. W.; Kim, G.-H.; Kim, J. Y. Functionalized PFN-X (X = Cl, Br, or I) for Balanced Charge Carriers of Highly Efficient Blue Light-Emitting Diodes. *ACS Appl. Mater. Interfaces* **2020**, *12*, 35740−35747.

(8) Senanayak, S. P.; Yang, B.; Thomas, T. H.; Giesbrecht, N.; Huang, W.; Gann, E.; Nair, B.; Goedel, K.; Guha, S.; Moya, X.; McNeill, C. R.; Docampo, P.; Sadhanala, A.; Friend, R. H.; Sirringhaus, H. Understanding Charge Transport in Lead Iodide Perovskite Thin-Film Field-Effect Transistors. *Sci. Adv.* **2017**, *3*, No. e1601935.

(9) Kang, K.; Ahn, H.; Song, Y.; Lee, W.; Kim, J.; Kim, Y.; Yoo, D.; Lee, T. High-Performance Solution-Processed Organo-Metal Halide Perovskite Unipolar Resistive Memory Devices in a Cross-Bar Array Structure. *Adv. Mater.* **2019**, *31*, No. 1804841.

(10) Gu, C.; Lee, J.-S. Flexible Hybrid Organic−Inorganic Perovskite Memory. *ACS Nano* **2016**, *10*, 5413−5418.

(11) Lee, D.; Hwang, B.; Lee, J.-S. Impact of Grain Sizes on Programmable Memory Characteristics in Two-Dimensional Organic−Inorganic Hybrid Perovskite Memory. *ACS Appl. Mater. Interfaces* **2019**, *11*, 20225−20231.

(12) Smith, I. C.; Hoke, E. T.; Solis-Ibarra, D.; McGehee, M. D.; Karunadasa, H. I. A Layered Hybrid Perovskite Solar-Cell Absorber with Enhanced Moisture Stability. *Angew. Chem.* **2014**, *126*, 11414−11417.

(13) Cao, D. H.; Stoumpos, C. C.; Farha, O. K.; Hupp, J. T.; Kanatzidis, M. G. 2D Homologous Perovskites as Light-Absorbing Materials for Solar Cell Applications. *J. Am. Chem. Soc.* **2015**, *137*, 7843−7850.

(14) Tsai, H.; Nie, W.; Blancon, J.-C.; Stoumpos, C. C.; Asadpour, R.; Harutyunyan, B.; Neukirch, A. J.; Verduzco, R.; Crochet, J. J.; Tretiak, S.; Pedesseau, L.; Even, J.; Alam, M. A.; Gupta, G.; Lou, J.; Ajayan, P. M.; Bedzyk, M. J.; Kanatzidis, M. G.; Mohite, A. D. High-Efficiency Two-Dimensional Ruddlesden−Popper Perovskite Solar Cells. *Nature* **2016**, *536*, 312−316.

(15) Hwang, B.; Lee, J. 2D Perovskite-Based Self-Aligned Lateral Heterostructure Photodetectors Utilizing Vapor Deposition. *Adv. Opt. Mater.* **2019**, *7*, No. 1801356.

(16) Stoumpos, C. C.; Cao, D. H.; Clark, D. J.; Young, J.; Rondinelli, J. M.; Jang, J. I.; Hupp, J. T.; Kanatzidis, M. G. Ruddlesden−Popper Hybrid Lead Iodide Perovskite 2D Homologous Semiconductors. *Chem. Mater.* **2016**, *28*, 2852−2867.

(17) Soe, C. M. M.; Nagabhushana, G. P.; Shivaramaiah, R.; Tsai, H.; Nie, W.; Blancon, J.-C.; Melkonyan, F.; Cao, D. H.; Traoré, B.; Pedesseau, L.; Kepenekian, M.; Katan, C.; Even, J.; Marks, T. J.; Navrotsky, A.; Mohite, A. D.; Stoumpos, C. C.; Kanatzidis, M. G. Structural and Thermodynamic Limits of Layer Thickness in 2D Halide Perovskites. *Proc. Natl. Acad. Sci. USA* **2019**, *116*, 58−66.

(18) Mitzi, D. B. Synthesis, Crystal Structure, and Optical and Thermal Properties of $(C_4H_9NH_3)_2MI_4$ (M = Ge, Sn, Pb). *Chem. Mater.* **1996**, *8*, 791−800.

(19) Mao, L.; Stoumpos, C. C.; Kanatzidis, M. G. Two-Dimensional Hybrid Halide Perovskites: Principles and Promises. *J. Am. Chem. Soc.* **2019**, *141*, 1171−1190.

(20) Soe, C. M. M.; Stoumpos, C. C.; Kepenekian, M.; Traoré, B.; Tsai, H.; Nie, W.; Wang, B.; Katan, C.; Seshadri, R.; Mohite, A. D.; Even, J.; Marks, T. J.; Kanatzidis, M. G. New Type of 2D Perovskites with Alternating Cations in the Interlayer Space, $(C(NH_2)_3)(CH_3NH_3)_nPb_nI_{3n+1}$: Structure, Properties, and Photovoltaic Performance. *J. Am. Chem. Soc.* **2017**, *139*, 16297−16309.

(21) Dong, R.; Lan, C.; Xu, X.; Liang, X.; Hu, X.; Li, D.; Zhou, Z.; Shu, L.; Yip, S.; Li, C.; Tsang, S.-W.; Ho, J. C. Novel Series of Quasi-2D Ruddlesden−Popper Perovskites Based on Short-Chained Spacer Cation for Enhanced Photodetection. *ACS Appl. Mater. Interfaces* **2018**, *10*, 19019−19026.

(22) Li, Z.; Liu, N.; Meng, K.; Liu, Z.; Hu, Y.; Xu, Q.; Wang, X.; Li, S.; Cheng, L.; Chen, G. A New Organic Interlayer Spacer for Stable and Efficient 2D Ruddlesden−Popper Perovskite Solar Cells. *Nano Lett.* **2019**, *19*, 5237−5245.

(23) Milić, J. V.; Im, J.; Kubicki, D. J.; Ummadisingu, A.; Seo, J.; Li, Y.; Ruiz-Preciado, M. A.; Dar, M. I.; Zakeeruddin, S. M.; Emsley, L.; Grätzel, M. Supramolecular Engineering for Formamidinium-Based Layered 2D Perovskite Solar Cells: Structural Complexity and Dynamics Revealed by Solid-State NMR Spectroscopy. *Adv. Energy Mater.* **2019**, *9*, No. 1900284.

(24) Alanazi, A. Q.; Kubicki, D. J.; Prochowicz, D.; Alharbi, E. A.; Bouduban, M. E. F.; Jahanbakhshi, F.; Mladenović, M.; Milić, J. V.; Giordano, F.; Ren, D.; Alyamani, A. Y.; Albrithen, H.; Albadri, A.; Alotaibi, M. H.; Moser, J.-E.; Zakeeruddin, S. M.; Rothlisberger, U.; Emsley, L.; Grätzel, M. Atomic-Level Microstructure of Efficient Formamidinium-Based Perovskite Solar Cells Stabilized by 5-Ammonium Valeric Acid Iodide Revealed by Multinuclear and Two-Dimensional Solid-State NMR. *J. Am. Chem. Soc.* **2019**, *141*, 17659−17669.

(25) Alharbi, E. A.; Alyamani, A. Y.; Kubicki, D. J.; Uhl, A. R.; Walder, B. J.; Alanazi, A. Q.; Luo, J.; Burgos-Caminal, A.; Albadri, A.; Albrithen, H.; Alotaibi, M. H.; Moser, J.-E.; Zakeeruddin, S. M.; Giordano, F.; Emsley, L.; Grätzel, M. Atomic-Level Passivation Mechanism of Ammonium Salts Enabling Highly Efficient Perovskite Solar Cells. *Nat. Commun.* **2019**, *10*, No. 3008.

(26) Ruiz-Preciado, M. A.; Kubicki, D. J.; Hofstetter, A.; McGovern, L.; Futscher, M. H.; Ummadisingu, A.; Gershoni-Poranne, R.; Zakeeruddin, S. M.; Ehrler, B.; Emsley, L.; Milić, J. V.; Grätzel, M. Supramolecular Modulation of Hybrid Perovskite Solar Cells via Bifunctional Halogen Bonding Revealed by Two-Dimensional $^{19}F$ Solid-State NMR Spectroscopy. *J. Am. Chem. Soc.* **2020**, *142*, 1645−1654.

(27) Quintero-Bermudez, R.; Gold-Parker, A.; Proppe, A. H.; Munir, R.; Yang, Z.; Kelley, S. O.; Amassian, A.; Toney, M. F.; Sargent, E. H. Compositional and Orientational Control in Metal Halide Perovskites of Reduced Dimensionality. *Nat. Mater.* **2018**, *17*, 900−907.

(28) Lee, H.; Kim, H.; Cho, H.; Cha, W.; Hong, Y.; Kim, Y.; Sadhanala, A.; Venugopalan, V.; Kim, J. S.; Choi, J. W.; Lee, C.; Kim, D.; Yang, H.; Friend, R. H.; Lee, T. Efficient Ruddlesden−Popper Perovskite Light-Emitting Diodes with Randomly Oriented Nanocrystals. *Adv. Funct. Mater.* **2019**, No. 1901225.

(29) Hoye, R. L. Z.; Schulz, P.; Schelhas, L. T.; Holder, A. M.; Stone, K. H.; Perkins, J. D.; Vigil-Fowler, D.; Siol, S.; Scanlon, D. O.; Zakutayev, A.; Walsh, A.; Smith, I. C.; Melot, B. C.; Kurchin, R. C.; Wang, Y.; Shi, J.; Marques, F. C.; Berry, J. J.; Tumas, W.; Lany, S.; Stevanović, V.; Toney, M. F.; Buonassisi, T. Perovskite-Inspired Photovoltaic Materials: Toward Best Practices in Materials Characterization and Calculations. *Chem. Mater.* **2017**, *29*, 1964−1988.




https://dx.doi.org/10.1021/acs.chemmater.0c04078
*Chem. Mater.* 2021, 33, 370−377

(30) Pecher, O.; Carretero-González, J.; Griffith, K. J.; Grey, C. P. Materials' Methods: NMR in Battery Research. *Chem. Mater.* **2017**, *29*, 213−242.
(31) Schmidt-Rohr, K.; Spiess, H. W. *Multidimensional Solid-State NMR and Polymers*; Academic Press: London, 2005; pp 1−12.
(32) Roiland, C.; Trippé-Allard, G.; Jemli, K.; Alonso, B.; Ameline, J.-C.; Gautier, R.; Bataille, T.; Le Polles, L.; Deleporte, E.; Even, J.; Katan, C. Multinuclear NMR as a Tool for Studying Local Order and Dynamics in $CH_3NH_3PbX_3$ (X = Cl, Br, I) Hybrid Perovskites. *Phys. Chem. Chem. Phys.* **2016**, *18*, 27133−27142.
(33) Franssen, W. M. J.; Kentgens, A. P. M. Solid−State NMR of Hybrid Halide Perovskites. *Solid State Nucl. Magn. Reson.* **2019**, *100*, 36−44.
(34) Franssen, W. M. J.; van Es, S. G. D.; Dervişoğlu, R.; de Wijs, G. A.; Kentgens, A. P. M. Symmetry, Dynamics, and Defects in Methylammonium Lead Halide Perovskites. *J. Phys. Chem. Lett.* **2017**, *8*, 61−66.
(35) Kim, H.; Kim, J. S.; Heo, J.-M.; Pei, M.; Park, I.-H.; Liu, Z.; Yun, H. J.; Park, M.-H.; Jeong, S.-H.; Kim, Y.-H.; Park, J.-W.; Oveisi, E.; Nagane, S.; Sadhanala, A.; Zhang, L.; Kweon, J. J.; Lee, S. K.; Yang, H.; Jang, H. M.; Friend, R. H.; Loh, K. P.; Nazeeruddin, M. K.; Park, N.-G.; Lee, T.-W. Proton-Transfer-Induced 3D/2D Hybrid Perovskites Suppress Ion Migration and Reduce Luminance Overshoot. *Nat. Commun.* **2020**, *11*, No. 3378.
(36) Southern, S. A.; Errulat, D.; Frost, J. M.; Gabidullin, B.; Bryce, D. L. Prospects for $^{207}$Pb Solid-State NMR Studies of Lead Tetrel Bonds. *Faraday Discuss.* **2017**, *203*, 165−186.
(37) Senocrate, A.; Moudrakovski, I.; Maier, J. Short-Range Ion Dynamics in Methylammonium Lead Iodide by Multinuclear Solid State NMR and $^{127}$I NQR. *Phys. Chem. Chem. Phys.* **2018**, *20*, 20043−20055.
(38) Ha, M.; Karmakar, A.; Bernard, G. M.; Basilio, E.; Krishnamurthy, A.; Askar, A. M.; Shankar, K.; Kroeker, S.; Michaelis, V. K. Phase Evolution in Methylammonium Tin Halide Perovskites with Variable Temperature Solid-State $^{119}$Sn NMR Spectroscopy. *J. Phys. Chem. C* **2020**, *124*, 15015−15027.
(39) Kubicki, D. J.; Prochowicz, D.; Salager, E.; Rakhmatullin, A.; Grey, C. P.; Emsley, L.; Stranks, S. D. Local Structure and Dynamics in Methylammonium, Formamidinium, and Cesium Tin(II) Mixed-Halide Perovskites from $^{119}$Sn Solid-State NMR. *J. Am. Chem. Soc.* **2020**, *142*, 7813−7826.
(40) Wang, M.; Wu, X.-P.; Zheng, S.; Zhao, L.; Li, L.; Shen, L.; Gao, Y.; Xue, N.; Guo, X.; Huang, W.; Gan, Z.; Blanc, F.; Yu, Z.; Ke, X.; Ding, W.; Gong, X.-Q.; Grey, C. P.; Peng, L. Identification of Different Oxygen Species in Oxide Nanostructures with $^{17}$O Solid-State NMR Spectroscopy. *Sci. Adv.* **2015**, *1*, No. e1400133.
(41) Leung, T. L.; Tam, H. W.; Liu, F.; Lin, J.; Ng, A. M. C.; Chan, W. K.; Chen, W.; He, Z.; Lončarić, I.; Grisanti, L.; Ma, C.; Wong, K. S.; Lau, Y. S.; Zhu, F.; Skoko, Ž.; Popović, J.; Djurišić, A. B. Mixed Spacer Cation Stabilization of Blue-Emitting *n*=2 Ruddlesden−Popper Organic−Inorganic Halide Perovskite Films. *Adv. Opt. Mater.* **2020**, *8*, No. 1901679.
(42) Zhou, N.; Huang, B.; Sun, M.; Zhang, Y.; Li, L.; Lun, Y.; Wang, X.; Hong, J.; Chen, Q.; Zhou, H. The Spacer Cations Interplay for Efficient and Stable Layered 2D Perovskite Solar Cells. *Adv. Energy Mater.* **2020**, *10*, No. 1901566.
(43) Chen, S.; Shen, N.; Zhang, L.; Zhang, L.; Cheung, S. H.; Chen, S.; So, S. K.; Xu, B. Understanding the Interplay of Binary Organic Spacer in Ruddlesden−Popper Perovskites toward Efficient and Stable Solar Cells. *Adv. Funct. Mater.* **2020**, *30*, No. 1907759.
(44) Leng, K.; Abdelwahab, I.; Verzhbitskiy, I.; Telychko, M.; Chu, L.; Fu, W.; Chi, X.; Guo, N.; Chen, Z.; Chen, Z.; Zhang, C.; Xu, Q.-H.; Lu, J.; Chhowalla, M.; Eda, G.; Loh, K. P. Molecularly Thin Two-Dimensional Hybrid Perovskites with Tunable Optoelectronic Properties Due to Reversible Surface Relaxation. *Nat. Mater.* **2018**, *17*, 908−914.
(45) Li, J.; Wang, J.; Ma, J.; Shen, H.; Li, L.; Duan, X.; Li, D. Self-Trapped State Enabled Filterless Narrowband Photodetections in 2D Layered Perovskite Single Crystals. *Nat. Commun.* **2019**, *10*, No. 806.
(46) Wang, K.; Wu, C.; Yang, D.; Jiang, Y.; Priya, S. Quasi-Two-Dimensional Halide Perovskite Single Crystal Photodetector. *ACS Nano* **2018**, *12*, 4919−4929.
(47) Hanrahan, M. P.; Men, L.; Rosales, B. A.; Vela, J.; Rossini, A. J. Sensitivity-Enhanced $^{207}$Pb Solid-State NMR Spectroscopy for the Rapid, Non-Destructive Characterization of Organolead Halide Perovskites. *Chem. Mater.* **2018**, *30*, 7005−7015.
(48) Ueda, T.; Shimizu, K.; Ohki, H.; Okuda, T. 13C CP/MAS NMR Study of the Layered Compounds $[C_6H_5CH_2CH_2NH_3]_2[CH_3NH_3]_{n-1}Pb_nI_{3n+1}$ (N=1, 2). *Z. Naturforsch. A* **1996**, *51*, 910−914.
(49) Kubicki, D. J.; Prochowicz, D.; Hofstetter, A.; Péchy, P.; Zakeeruddin, S. M.; Grätzel, M.; Emsley, L. Cation Dynamics in Mixed-Cation $(MA)_x(FA)_{1-x}PbI_3$ Hybrid Perovskites from Solid-State NMR. *J. Am. Chem. Soc.* **2017**, *139*, 10055−10061.
(50) Shi, E.; Deng, S.; Yuan, B.; Gao, Y.; Akriti; Yuan, L.; Davis, C. S.; Zemlyanov, D.; Yu, Y.; Huang, L.; Dou, L. Extrinsic and Dynamic Edge States of Two-Dimensional Lead Halide Perovskites. *ACS Nano* **2019**, *13*, 1635−1644.
(51) Blancon, J.-C.; Tsai, H.; Nie, W.; Stoumpos, C. C.; Pedesseau, L.; Katan, C.; Kepenekian, M.; Soe, C. M. M.; Appavoo, K.; Sfeir, M. Y.; Tretiak, S.; Ajayan, P. M.; Kanatzidis, M. G.; Even, J.; Crochet, J. J.; Mohite, A. D. Extremely Efficient Internal Exciton Dissociation through Edge States in Layered 2D Perovskites. *Science* **2017**, *355*, 1288−1292.
(52) Feng, J.; Gong, C.; Gao, H.; Wen, W.; Gong, Y.; Jiang, X.; Zhang, B.; Wu, Y.; Wu, Y.; Fu, H.; Jiang, L.; Zhang, X. Single-Crystalline Layered Metal-Halide Perovskite Nanowires for Ultrasensitive Photodetectors. *Nat. Electron.* **2018**, *1*, 404−410.
(53) Bakulin, A. A.; Selig, O.; Bakker, H. J.; Rezus, Y. L. A.; Müller, C.; Glaser, T.; Lovrincic, R.; Sun, Z.; Chen, Z.; Walsh, A.; Frost, J. M.; Jansen, T. L. C. Real-Time Observation of Organic Cation Reorientation in Methylammonium Lead Iodide Perovskites. *J. Phys. Chem. Lett.* **2015**, *6*, 3663−3669.
(54) Fabini, D. H.; Seshadri, R.; Kanatzidis, M. G. The Underappreciated Lone Pair in Halide Perovskites Underpins Their Unusual Properties. *MRS Bull.* **2020**, *45*, 467−477.
(55) Fabini, D. H.; Laurita, G.; Bechtel, J. S.; Stoumpos, C. C.; Evans, H. A.; Kontos, A. G.; Raptis, Y. S.; Falaras, P.; Van der Ven, A.; Kanatzidis, M. G.; Seshadri, R. Dynamic Stereochemical Activity of the $Sn^{2+}$ Lone Pair in Perovskite $CsSnBr_3$. *J. Am. Chem. Soc.* **2016**, *138*, 11820−11832.
(56) Zhao, P.; Prasad, S.; Huang, J.; Fitzgerald, J. J.; Shore, J. S. Lead-207 NMR Spectroscopic Study of Lead-Based Electronic Materials and Related Lead Oxides. *J. Phys. Chem. B* **1999**, *103*, 10617−10626.
(57) Mehring, M. *Principles of High Resolution NMR in Solids*; Springer-Verlag, 1983.
(58) Taylor, R. E.; Beckmann, P. A.; Bai, S.; Dybowski, C. $^{127}$I and $^{207}$Pb Solid-State NMR Spectroscopy and Nuclear Spin Relaxation in $PbI_2$: A Preliminary Study. *J. Phys. Chem. C* **2014**, *118*, 9143−9153.
(59) Palosz, B. The Structure of $PbI_2$ Polytypes 2H and 4H: A Study of the 2H-4H Transition. *J. Phys. Condens. Matter* **1990**, *2*, 5285−5295.
(60) Fayon, F.; Farnan, I.; Bessada, C.; Coutures, J.; Massiot, D.; Coutures, J. P. Empirical Correlations between $^{207}$Pb NMR Chemical Shifts and Structure in Solids. *J. Am. Chem. Soc.* **1997**, *119*, 6837−6843.
(61) Xue, X.; Stebbins, J. F. $^{23}$Na NMR Chemical Shifts and Local Na Coordination Environments in Silicate Crystals, Melts and Glasses. *Phys. Chem. Miner.* **1993**, *20*, 297−307.
(62) Lee, S. K.; Stebbins, J. F. The Distribution of Sodium Ions in Aluminosilicate Glasses: A High-Field Na-23 MAS and 3Q MAS NMR Study. *Geochim. Cosmochim. Acta* **2003**, *67*, 1699−1709.
(63) Dawson, D. M.; Moran, R. F.; Ashbrook, S. E. An NMR Crystallographic Investigation of the Relationships between the Crystal Structure and $^{29}$Si Isotropic Chemical Shift in Silica Zeolites. *J. Phys. Chem. C* **2017**, *121*, 15198−15210.

(64) Viger-Gravel, J.; Leclerc, S.; Korobkov, I.; Bryce, D. L. Correlation between 13C Chemical Shifts and the Halogen Bonding Environment in a Series of Solid Para-Diiodotetrafluorobenzene Complexes. *CrystEngComm* **2013**, *15*, 3168.
(65) Yesinowski, J. P.; Eckert, H.; Rossman, G. R. Characterization of Hydrous Species in Minerals by High-Speed Proton MAS-NMR. *J. Am. Chem. Soc.* **1988**, *110*, 1367−1375.
(66) Viger-Gravel, J.; Meyer, J. E.; Korobkov, I.; Bryce, D. L. Probing Halogen Bonds with Solid-State NMR Spectroscopy: Observation and Interpretation of J($^{77}$Se, $^{31}$P) Coupling in Halogen-Bonded P═Se···I Motifs. *CrystEngComm* **2014**, *16*, 7285−7297.
(67) Febriansyah, B.; Koh, T. M.; Rana, P. J. S.; Hooper, T. J. N.; Ang, Z. Z.; Li, Y.; Bruno, A.; Grätzel, M.; England, J.; Mhaisalkar, S. G.; Mathews, N. Hybrid 2D $[Pb(CH_3NH_2)I_2]_n$ Coordination Polymer Precursor for Scalable Perovskite Deposition. *ACS Energy Lett.* **2020**, 2305−2312.
(68) Cattaneo, A. S.; Ferrara, C.; Marculescu, A. M.; Giannici, F.; Martorana, A.; Mustarelli, P.; Tealdi, C. Solid-State NMR Characterization of the Structure and Thermal Stability of Hybrid Organic−Inorganic Compounds Based on a $HLaNb_2O_7$ Dion−Jacobson Layered Perovskite. *Phys. Chem. Chem. Phys.* **2016**, *18*, 21903−21912.
(69) Zhao, S.; Lan, C.; Li, H.; Zhang, C.; Ma, T. Aurivillius Halide Perovskite: A New Family of Two-Dimensional Materials for Optoelectronic Applications. *J. Phys. Chem. C* **2020**, *124*, 1788−1793.
(70) Pell, A. J.; Clément, R. J.; Grey, C. P.; Emsley, L.; Pintacuda, G. Frequency-Stepped Acquisition in Nuclear Magnetic Resonance Spectroscopy under Magic Angle Spinning. *J. Chem. Phys.* **2013**, *138*, No. 114201.
(71) Bak, M.; Rasmussen, J. T.; Nielsen, N. C. SIMPSON: A General Simulation Program for Solid-State NMR Spectroscopy. *J. Magn. Reson.* **2000**, *147* (2), 296−330.


https://dx.doi.org/10.1021/acs.chemmater.0c04078
*Chem. Mater.* 2021, 33, 370−377